Incorporation of aerosols into the COSPv2 satellite lidar simulator for climate model evaluation

Marine Bonazzola[1], Hélène Chepfer[1], Po-Lun Ma[2], Johannes Quaas[3], David Winker[4], Artem Feofilov[1] and Nick Schutgens[5]

[1] Laboratoire de Météorologie Dynamique, École Polytechnique, Palaiseau, France
[2] Pacific Northwest National Laboratory, Richland, WA, USA
[3] Institute for Meteorology, Universität Leipzig, Leipzig, Germany
[4] Nasa Langley Research center, Hampton, Virginia, USA
[5] Vrije Universiteit, Amsterdam, Netherlands
Correspondence to : Marine Bonazzola (marine.bonazzola@gmail.com)

Abstract Aerosols have a large impact on climate, air quality, and biogeochemical cycles. Their concentrations are highly variable in space and time, and a key variability is in their vertical distribution, because it influences atmospheric heating profiles, aerosols life-time and, as a result, surface concentrations, and because it has an impact on aerosol-cloud interactions. On the side of model-oriented aerosols research, using a lidar aerosol simulator ensures consistent comparisons between the modeled aerosols and the observed aerosols. In the current study, we present the lidar aerosol simulator implemented within the COSPv2 satellite lidar simulator. We estimate the attenuated total backscattered signal (ATB) and the backscatter ratios (SR) that would be observed at 532 nm by the lidar CALIOP over-flying the atmosphere predicted by the E3SMv1 climate model. The simulator performs the computations at the same vertical resolution as the CALIOP lidar, making use of aerosol optics from the E3SMv1 model as inputs, and assuming that aerosols are uniformly distributed horizontally within each model grid-box. It applies a cloud masking and an aerosol detection threshold, to get the ATB and SR profiles that would be observed above clouds by CALIOP with its actual aerosol detection capability. Our comparison shows that the aerosol distribution simulated at a seasonal timescale is generally in good agreement with observations, with however a discrepancy in the Southern Hemisphere, as the observed SR maximum is not reproduced in simulations there. Comparison between cloud-screened and non cloud-screened computed SRs shows little differences, indicating that the cloud screening by potentially incorrect model clouds does not affect the mean aerosol signal averaged over a season. Consequently, the differences between observed and simulated SR values are not due to sampling errors, and allow to point out some weaknesses in the aerosol representation in models. The use of lidar observations at several wavelengths can give further indication on the nature of the aerosols that need to be improved.

1. Motivation

The role of aerosols in the Earth system has been recognized as a major source of uncertainty for decades. Aerosols have significant impacts on the climate system, as well as on weather and air quality,

and Earth's biogeochemical cycles (Szopa et al., 2021). They modulate the Earth's energy budget via aerosol-radiation and aerosol-cloud interactions, exerting radiative forcings to the climate system (Forster et al., 2021). They also affect the Earth's water cycle by changing clouds and precipitation characteristics (Douville et al., 2021). Due to their short lifetime (up to several days in the troposphere) compared to greenhouse gases, aerosols are highly variable in space and time. Obtaining appropriate information about the spatiotemporal distribution of aerosols from satellite measurements remains a key challenge (Constantino and Bréon, 2013).

Passive satellite measurements have been used to study column-integrated properties of aerosols, but they are not suited for the vertical distribution of aerosols. Nevertheless, aerosol vertical distribution is critical when it comes to aerosol-radiation interactions (Zarzycki and Bond, 2010). This in particular applies to the adjustments to aerosol-radiation interactions or semi-direct effect, where the vertical alignment of clouds and aerosols is crucial (Koch and Del Genio, 2010). Aerosol vertical distribution also affects aerosols lifetime (e.g. Keating and Zuber, 2007) and aerosol-cloud interactions (e.g. Waquet et al. 2009; Stier, 2016; Quaas et al., 2020).

Space-borne lidars fill this gap by providing detailed information about the vertical distribution of aerosols. This is particularly useful for studying long-range transport of smoke or dust in the free troposphere and stratosphere, and for studying the interactions between aerosols and ice clouds in the upper troposphere, because the vertically integrated aerosols quantities retrieved from passive sensors are mostly about aerosols in the planetary boundary layer. Furthermore, space lidars can retrieve aerosols in regions where the surface is reflective, such as the polar regions and desert, while passive satellite instruments only have limited capabilities retrieving aerosols in those conditions. Over the last decade, the aerosol profiles collected by space lidars have contributed to progress on a variety of aerosols research (https://www-calipso.larc.nasa.gov/).

Vertical profiles of aerosols observed by space lidar (e.g. Winker et al. 2013) have also been used to evaluate the models (Koffi et al., 2012; 2016). More advanced comparisons between model and lidar observations have demonstrated the value of using a lidar aerosol simulator to ensure consistent comparisons between the modeled aerosols and the observed aerosols (Ma et al. 2018, Hodzic et al. 2004, Watson-Parris et al. 2018). In parallel, the cloud community has developed satellite simulators to establish a closer bridge between observed and modeled clouds and facilitate the use of space-based data by the model community for a variety of topics such as evaluating the model physics, studying climate feedbacks, inter-comparing several models in a consistent way over short-term and long-term simulations. In particular, the active sensor satellite simulators developed for lidars and radars have been proven to be useful tools to properly take into account the limits of this type of observations (eg. cloud masking, signal-to-noise ratio, sub-gridding) when comparing observations and models.

These previous works suggest that a closer bridge between aerosols observations from space lidars and models could be beneficial in the context of three different configurations of simulations : the nudged simulations, atmospheric simulations with prescribed sea surface temperature (SST), and fully coupled Earth system model simulations.

First, the constraints of 15 years of Cloud-Aerosol Lidar and Infrared Pathfinder Satellite Observations (CALIPSO) (2006-2020) on aerosol vertical distribution would be useful to improve the aerosol transport processes and aerosol removal processes in models, when those observations are compared to the simulated aerosol in nudged simulations where e.g. winds are relaxed towards reanalyses. On the other hand, using observational constraints together with a climatology statistic approach of simulations with prescribed SST can be beneficial to account for circulation feedbacks to aerosol forcing. Indeed, while the transport by large-scale circulation determines the geographical patterns of aerosol forcing, this aerosol forcing also impacts large-scale circulation, as it can be characterized by aerosol optical depths (AOD) retrieved by MODerate resolution Imaging Spectroradiometer (MODIS) or VIsible Infrared Imaging Radiometer Suite (VIIRS). Finally, long-term (100 years) simulations of the coupled ocean-atmosphere system (control and RCP8.5 type simulations) can help to understand the role of aerosol in the context of climate change.

The lidar simulator translates the vertical profiles of aerosol extinction and backscatter coefficients computed by a model into vertical profiles of the two key variables retrieved by a lidar : the attenuated total backscatter, and the backscatter ratio. These two lidar variables are derived online within the model, to account for the 2-way attenuation within the light's transmittance along its path from the laser to the scattering object, and the return-path back to the detector, the calculations also accounting for the molecular backscatter (i.e. Rayleigh backscatter), calculated from the model's air temperature and pressure profiles. Furthermore the model is sampled on the satellite orbital path, the fully overcast cases are masked out to take account of the impossibility for a space lidar to observe aerosols below optically thick clouds, and only the signal above the instrumental noise is retained.

We incorporate modules included in previously developed simulators (Ma et al. 2018, Vuolo et al. 2009, Hodzic et al. 2004) into the community tool CFMIP Observation Simulator Package (COSP) to create a simple base on which each group can build up its own analysis. The goal is to facilitate the comparison between GCMs and space lidar aerosols data. Besides CALIPSO operating at 532 nm and 1064 nm, the ATmospheric LIDar (ATLID) instrument of the EarthCARE mission is expected to become operational in 2023. In synergy with other instruments, it will provide vertical profiles of aerosols and thin clouds, operating at 355 nm with a high-spectral resolution (HSR) receiver and depolarization channel. Later on another HSR Lidar operating at 532 nm and 1064 nm is expected to be launched. The COSPv2 lidar simulator will thus be a useful tool for the exploitation of these new datasets and the comparison with General Circulation Models (GCMs) of several modeling groups.

We choose to implement the lidar aerosol simulator within the COSPv2 infrastructure because COSPv2 infrastructure already contains several capabilities (from the cloud lidar simulator but not only) that can be re-used for the lidar aerosol simulator. Moreover, COSPv2 is already implemented in several GCMs (Webb et al. 2019) so the addition of the lidar aerosol simulator module requires only minimum effort for the modeling groups.

2. Concept and Design
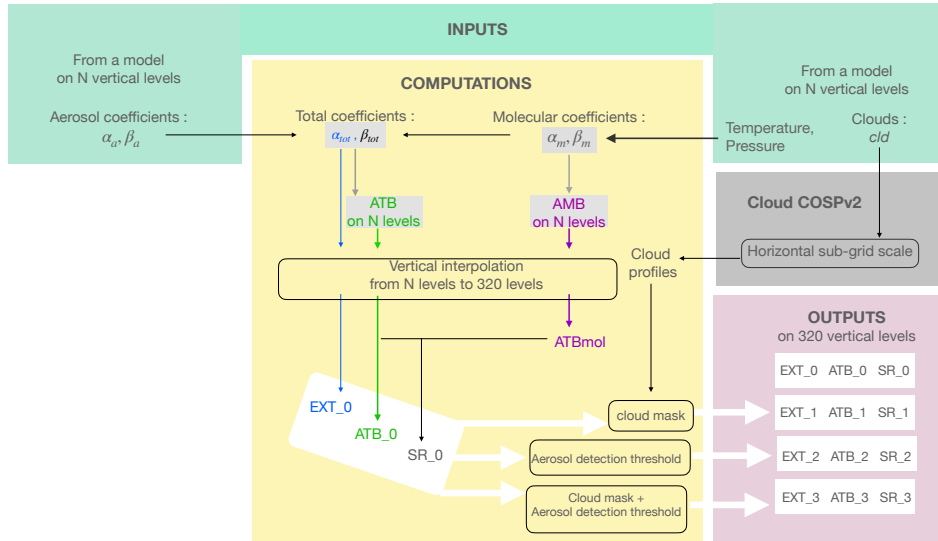
Figure 1 : Schematic of the lidar aerosol COSPv2 simulator. The logical variable to be set to "true" for the use of the aerosol simulator is : lidar_aerosols, use_vgrid_aerosols. The logical variable use_obs_for_aerosols must be set to "false". The number of vertical levels for aerosols has to be defined (in the current study, nlvgrid_aersols = 320).

1 The aerosol simulator described in this section mimics the aerosol observations that would be observed
2 by a space lidar overflying the atmosphere predicted by the model (Fig. 1). Hereafter we first define the
3 usual aerosol variables (specifically, the attenuated total backscattered signal ATB and the backscatter
4 ratio SR). Then we describe the main steps of the lidar aerosol simulator. Finally we discuss its
5 implementation and its main differences with the cloud lidar simulator.

6
7
2.1 Definitions
8
9 As defined by e.g. Stromatas et al. (2012), the attenuated total backscattered signal (in m^{-1} sr^{-1})
10 represents the signal backscattered towards the lidar by aerosols and molecules, and attenuated along
11 its path by aerosols and molecules in a cloud-free atmosphere. It is given by :
12
13 $ATB = (\beta_m(\lambda, z) + \beta_a(\lambda, z)) \cdot exp[-2 \int_z^{TOA} (\alpha_m(\lambda, z') + \alpha_a(\lambda, z'))dz']$, where β_m and β_a are the
14
15 molecule and aerosol 180º backscatter profiles (in m^{-1} sr^{-1}), respectively ; α_m and α_a are the extinction
16 coefficients for molecules and aerosols (in m^{-1}), respectively, and TOA denotes the top of the
17 atmosphere.
18 The 180º Rayleigh/molecular backscatter coefficient depends on temperature (in K), pressure (in Pa)
19 and on the wavelength λ (in μm) : $\beta_m = \frac{P}{kT}(5.45 \times 10^{-32})(\frac{\lambda}{0.55})^{-4.09}$, where k is the Boltzmann
20
21 constant (k=$1.38 \times 10^{-23} JK^{-1}$). The extinction coefficient by molecules can be simply expressed as :
22
23 $\alpha_m = \frac{\beta_m}{0.119}$.

The 180° backscatter and extinction coefficients for aerosols depend on the microphysical properties of the particles (their size distribution, shape and phase), and on the refraction index of the medium, that depends on the aerosol chemical composition.

To highlight aerosols in an atmospheric layer versus molecular background, one often uses the backscatter ratio (SR). The definition of SR used in CALIPSO products (e.g. Chepfer et al. 2008, 2013) is : $SR(\lambda, z) = \dfrac{ATB}{AMB}$, where AMB is the attenuated molecular backscattered signal in the absence of

aerosols : $AMB(\lambda, z) = \beta_m(\lambda, z) \cdot exp[-2\int_{z}^{TOA} \alpha_m(\lambda, z')dz']$. Therefore $SR = 1$ in absence of

aerosols (molecules only).

2.2 Concept

The GCM provides pressure, temperature and cloud fraction at each level and for each latitude-longitude grid cell. When the GCM includes an interactive aerosol module, it also provides on this 3D -grid the optical properties of aerosols at a given wavelength, that depend on the specific GCM parameterizations, *ie* the nature of the modeled aerosols, the chosen aerosol size distributions etc. The optical properties computed by the GCM can be directly the extinction and 180° backscatter aerosol coefficients ; depending on the GCM they might also be the simple scattering albedo, the phase function and the absorption coefficient. In the latter case, the modeling centers are required to implement additional computation to convert these optical properties into the aerosol extinction and 180° backscatter coefficients, that are needed as inputs of the lidar simulator. These coefficients must be defined at a given wavelength : 532 nm for CALIPSO/Cloud-Aerosol LIdar with Orthogonal Polarization (CALIOP). Optical properties at 532 nm are standard outputs for most GCMs. Coefficients defined at other wavelengths, *e.g.* 1064 nm for CALIOP or 355nm for EarthCare/ATLID, may also be added as inputs for additional diagnostics.

 In the steps listed below, it is assumed that the process applies to a vertical profile, and that it is repeated for all longitude-latitude grid cells and for each time step of the GCM.

1) First, the ACTSIM procedure already implemented in COSP calculates the $\alpha_M(z), \beta_m(z)$ and $AMB(z)$ vertical profiles using the GCM pressure and temperature profiles, according to the equations of Section 2.1. The GCM vertical profile of cloud fraction is also transmitted to the procedure SCOPS of COSPv2, that performs a subgridding within the grid cell and defines the vertical column of grid cells as being 100% overcast or not.

2) The Attenuated Total Backscatter (ATB) profile and backScatter Ratio (SR) profile are computed at model levels. These variables are calculated according to the equations of Section 2.1, using the input variables α_a and β_a and the variables α_m, β_m and AMB calculated in Step 1.

3) The total extinction ($\alpha_a + \alpha_m$), the (ATB) and the (SR) profiles are vertically re-gridded over a standard vertical grid having N equidistant levels to obtain profiles of total extinction (EXT_0),

attenuated total backscatter (ATB_0) and backscatter ratio (SR_0) at the vertical resolution of the space lidar observations that would be observed in absence of instrumental noise. For comparison with CALIPSO observations, N is set to 320 levels so each level is 60m thick from the bottom to 19,17 km of altitude. N is parameterized in the simulator so that it can be adapted to others lidars (eg. ATLID/EarthCare will have a 100m vertical resolution).

4) The aerosol detection thresholds, based on the actual space lidar capability (above instrumental noise) are applied to the EXT_0, ATB_0 and SR_0 profiles, in order to get the profiles of total extinction (EXT_2), attenuated total backscatter (ATB_2) and backscatter ratio (SR_2) that would be observed by a space lidar overflying the atmosphere predicted by the model in absence of clouds. This takes into account the limited capability to detect aerosols when the signal-to-noise ratio is too low for CALIPSO. The aerosol detection threshold is set to 1.2 in the current study but it is parameterized so that it can be easily adapted to other future space lidars depending on their signal-to-noise-ratio (SNR) which depends on the instrument itself.

5) The cloud masking is applied to the initial profiles EXT_0, ATB_0 and SR_0 to get the total extinction (EXT_1), attenuated total backscatter (ATB_1), and backscatter ratio (SR_1) profiles that would be observed above clouds by a space lidar with a perfect aerosol detection capability (no instrumental noise). This takes into account the impossibility of a space lidar to observe aerosols below clouds with optical depth larger than typically 3 to 5 - depending on the cloud microphysics – because the laser beam is fully attenuated. The cloud masking is built from the modeled clouds (not the actual clouds) as it would be seen by a space lidar. It is taken from the cloud lidar simulator output called Cloud Fraction profiles (CF3D). When scanning each grid point from the TOA to the surface, the first altitude level where CF3D=1 is called "z_bottom" and all aerosol-related output values at that altitude and below are set to Fill_value.

6) The cloud masking (step 5) and aerosol detection thresholds (step 4) are applied to the initial profiles (EXT_0, ATB_0 and SR_0) to get the total extinction (EXT_3), the attenuated total backscatter (ATB_3), and backscatter ratio (SR_3) profiles that would be observed above clouds by a space lidar with actual aerosol detection capability.

2.3 Differences between the CALIPSO Aerosol and Cloud Simulators

The aerosol lidar simulator is implemented within the COSPv2 infrastructure. Indeed this latter already contains a cloud lidar simulator from which several routines are used within the aerosol lidar simulator, moreover COSPv2 is time-optimized to run over long time scales (hundred years) when needed. The main differences between the aerosol lidar simulator presented in this paper and the cloud lidar simulator (Chepfer et al. 2008, Cesana and Chepfer, 2012, 2013, Guzman et al. 2017, Reverdy et al. 2015) already implemented in COSPv2 are the followings:

1) The aerosol lidar simulator needs aerosol optics from the models as inputs (α_a and β_a profiles in each model grid boxes) because those are strongly model dependent for aerosols while they are not for clouds. Indeed, the cloud particles are much larger than the lidar wavelength, which makes the cloud

optical properties more simple than the aerosols ones at the lidar wavelengths (visible, UV, near IR), and clouds do not have the chemical complexity of aerosols.

2) Within the aerosol lidar simulator the aerosol-related computations are performed in each grid-box (typically of order of 1°x1°), while the cloud simulator computations are performed at a sub-grid scale (typically 50 sub-grid boxes in a grid box). Indeed the aerosols spatial structure is more homogeneous than that of the clouds in the atmosphere, hence we do not describe sub-grid aerosol variability. This approach implies that at a given level of altitude, we assume that aerosols are uniformly distributed horizontally within a grid-box while clouds are not.

3) The aerosol lidar simulator uses a more detailed vertical grid than the cloud simulator : eg. 320 vertical levels (typically 60m) instead of 40 (typically 480m), because the detailed vertical structure is important for aerosol emission height and transport especially in the atmospheric boundary layer. Note that, for clouds the vertical resolution used in CFMIP experiments (480m) results from a compromise between the wish to keep high horizontal resolution for sparse shallow clouds, the SNR of CALIPSO data in day time and the vertical resolution of CloudSat.

The user can choose to run the new aerosol routine alone, or the standard cloud routines alone (default), or both. These new features are controlled by two new keys in the user's configuration file in COSPv2 code (cf Figure 1).

3. Observations

Here we build an observational dataset consistent with the model+aerosol lidar simulator outputs SR_3 and ATB_3, that are the SR and ATB profiles observed above clouds by the CALIPSO lidar as described in the previous section. Note that contrary to SR_3 and ATB_3, the total extinction profile (EXT_3) cannot be observed directly by CALIPSO, it is an output from the simulator to support the interpretation of the difference between the observation and the model+simulator outputs.

We use the CALIPSO L1.5 orbit file (https://www-calipso.larc.nasa.gov/resources/calipso_user-s_guide/qs/cal_lid_l15_v1-00.php) dataset that contains cloud screened ATB profiles at 532nm with 60m vertical resolution and 20km long-track horizontal resolution, 90m cross-track. The CALIPSO L1.5 data are built from the native L1 CALIPSO data (1/3km horizontal resolution long-track, 90m cross-track and 30m vertical) on which cloud screening is applied iteratively at different horizontal resolutions from 1/3km up to 80km, so that all the cloudy levels of each 1/3km profile are screened and all the cloud-free level of each 1/3km profile are retained below the altitude of 8 km. Then, the cloud-free levels of the successive 1/3km profiles are averaged horizontally along 20km to get the CALIPSO L1.5 profiles. As each L1.5 20km profile represents an average signal over the cloud-free levels along these 20km, it cannot be used to study aerosols horizontal heterogeneities smaller than 20km. But it presents the advantage of having a much higher SNR than the original L1 profile (1/3km) which permits the use of the lower aerosol detectability threshold in both observations and simulations, and the detection of optically thin aerosol layers assuming they are homogeneously distributed spatially along 20km.

For the current study, we build a gridded product consistent with the model+aerosol lidar simulator outputs, in averaging all the L1.5 ATB cloud-screened profiles falling into a 1°x1° grid box at a given date. Given the CALIPSO polar orbit, the number of profiles is larger at high latitudes than in the tropics where not all the grid boxes contain a satellite observation each day.

Similarly, we build the SR gridded product from the orbit L1.5 ATB dataset. To do so, we first compute the AMB profiles - the signal that would be measured by the lidar in a cloud-free and aerosol-free atmosphere - at 20km along track resolution, 60m vertical, from the GMAO pressure and temperature profiles included in L1.5 data using the lidar equation. Then we compute the SR profiles by dividing the L1.5 ATB with AMB. Finally we average all the 20km-SR profiles within the 1°x1° gidbox. Note that it is better to compare the observed and simulated SR profiles rather than the observed and simulated ATB profiles, because the model SR profile is normalized against the model pressure and temperature profiles and the observed SR profile is normalized against the pressure and temperature from GMAO re-analysis.

In the upper troposphere where AMB and ATB values are low, the 1°x1° ATB profiles measured along the orbit still have low signal to noise ratios that artificially induce high values of SR. We thus process the data to filter out the noise, by setting ATB=AMB when ATB-AMB is lower than 1e-4 km^{-1} sr^{-1} and SR=1 when SR is lower than 1.2. The threshold on AMB typically applies above 8 km. Both threshold values are relevant for night profiles, that are less noisy than daily ones. We thus focus in this study on profiles observed at night only, before and after the application of the AMB/SR thresholds. Note that the threshold on SR is parameterized in the aerosol simulator and can be easily adapted to other times of the day or to other instruments.

Finally, to compare the observations with the model+simulator outputs, the gridded data long-track are averaged daily, and then monthly. The comparison is thus possible at three different time and space scales : 1) the orbit files of SR profiles at 1° horizontal resolution along-track, 60m vertical and instantaneous time scale 2) the 3D daily 1°x1° gridded SR profiles, 60m vertical resolution, which differ from those of the orbit files poleward of 70°, and in cells where day and nigh orbits cross 3) the 3D monthly 1°x1° gridded SR profiles, 60m vertical resolution.

4. Examples of outputs of the COSPv2/Lidar-Aerosols simulator

4.1 Orbit files

We consider the attenuated total backscatter profiles observed by CALIPSO at 532 nm along its trajectory on 20 March 2008 (arbitrarily chosen), before and after the application of the AMB/SR thresholds. These profiles, characterized by their latitude in Figures 2a and 2c, show missing values below the clouds with sufficient optical thickness to fully attenuate the laser beam. Such clouds occur at very high altitudes within the tropics, making it impossible to retrieve significant signals below 17 km at some locations. In dry regions (e.g., between 10°N and 30°N, 20°S and 40°S) however, the absence of clouds allows the lidar to retrieve entire ATB profiles down to the surface. The attenuated total backscatter
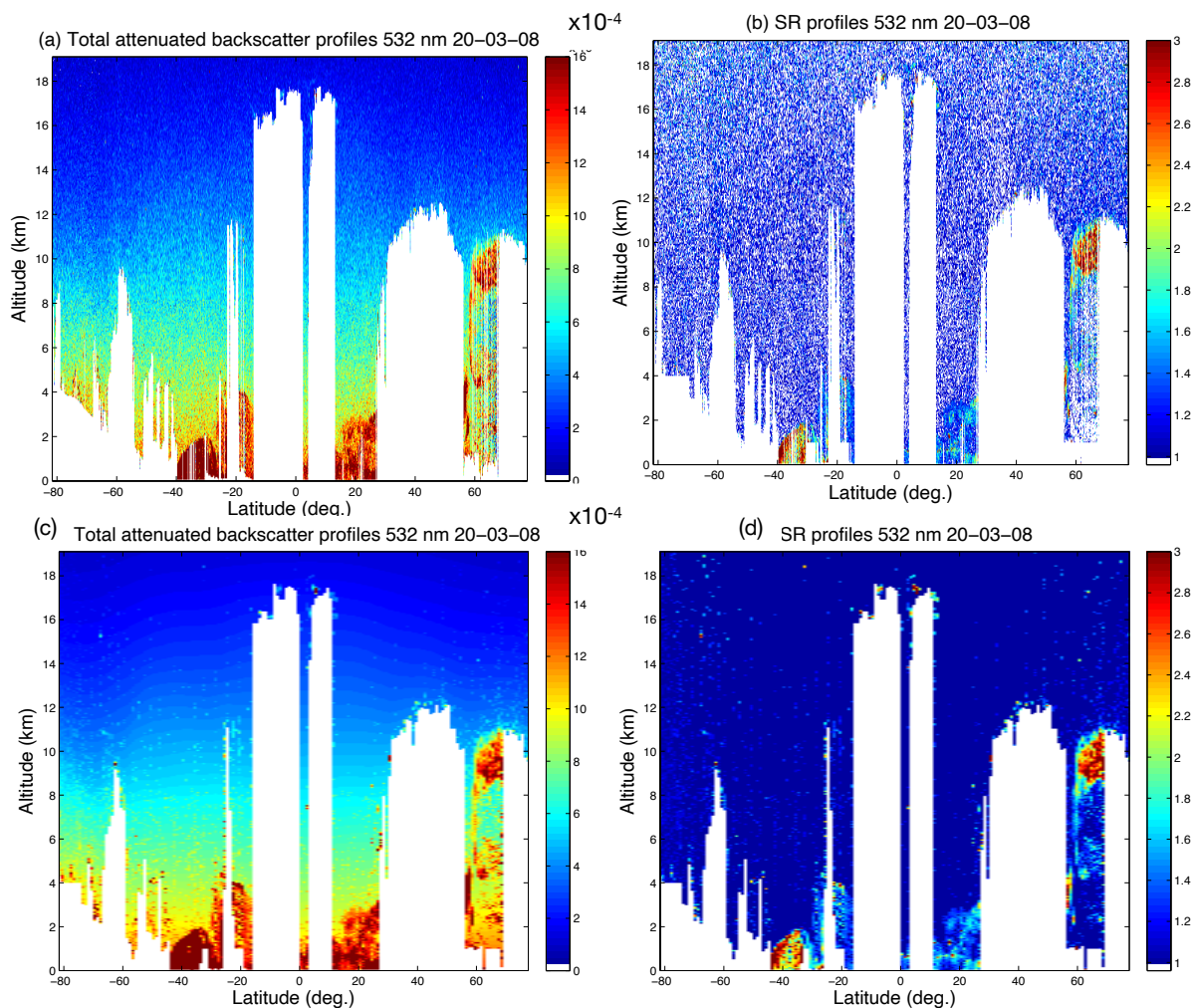
Figure 2 : Attenuated total backscatter profiles (km⁻¹sr⁻¹) before noise filtering (a) and after noise filtering (c); backscatter ratio profiles before noise filtering (b) and after noise filtering (d); observed by CALIOP at 532 nm along the satellite orbit on the 20-03-2008.

signal, that contains the molecular backscatter signal, shows a maximum near the surface, with a monotonic decrease as altitude increases. The SR profiles (Figures 2b and 2d), being normalized by the molecular signal, filter out the contribution by air molecules and are thus more appropriate to retrieve aerosol concentrations. A large amount of SR values that were initially lower than 1 because of the instrument noise (Figure 2b) are set to 1 by the application of the AMB/SR thresholds (Figure 2d). The SR profiles show maxima that are generally located below 4 km along the orbit. In the polar region in the Northern Hemisphere, however, a maximum is found between 10 km and 12 km, that might be attributable to polluted dust. Another maximum clearly appears in the lower troposphere at 30°S.

In Figure 3, we show the results of the U.S. Department of Energy's Energy Exascale Earth System Model version 1 (E3SMv1) (Golaz et al. 2019). The model is configured to run with prescribed SST and sea ice extent. The E3SM atmosphere model version 1 (EAMv1) (Rash et al. 2019) model outputs are used to compute the ATB and SR profiles that would be seen by the lidar along its trajectory on the
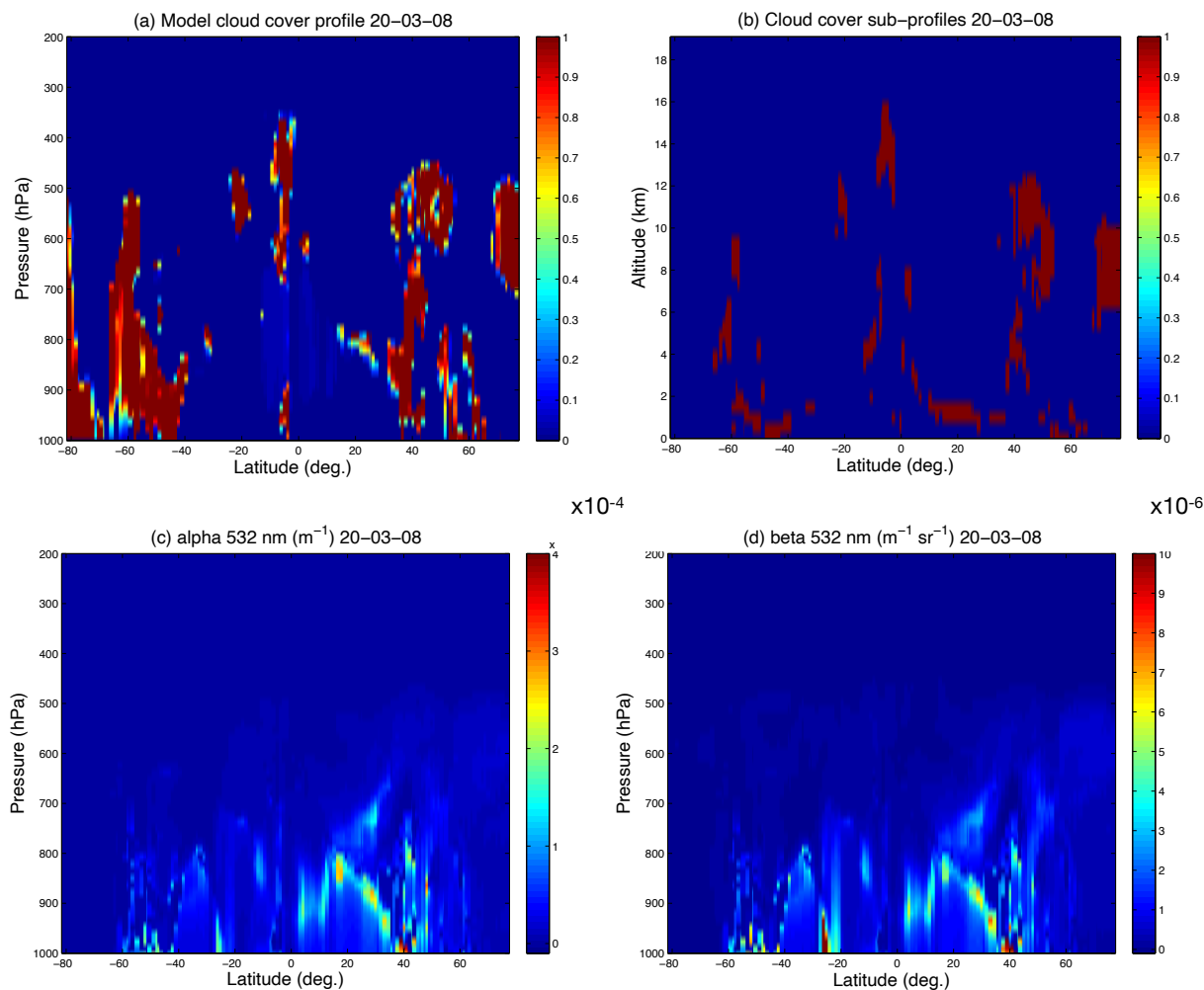
9

Figure 3 : (a) Vertical profiles of cloud fraction simulated by the E3SMv1 model along the satellite orbit on the 20-03-2008; (b) Same vertical profiles, defined by the COSPv2 simulator at the sub-grid scale and interpolated on 40 vertical levels; (c) Aerosol extinction profiles (in m-1) and (d) Aerosol backscatter coefficient profiles (in m-1 sr-1) calculated by E3SMv1 along the satellite orbit.

same date (20 March 2008). The model horizontal winds are nudged towards Modern-Era Retrospective analysis for Research and Applications version 2 (MERRA-2) (Gelaro et al. 2017) reanalysis with a relaxation time scale of 6 hours (Zhang et al., 2014 ; Ma et al., 2015). The simulated cloud vertical profiles (Figure 3a) agree very well with the observations (Figure 2), as high cloud fractions along the satellite trajectory coincide with the horizontal locations and altitudes of missing data in the observations.
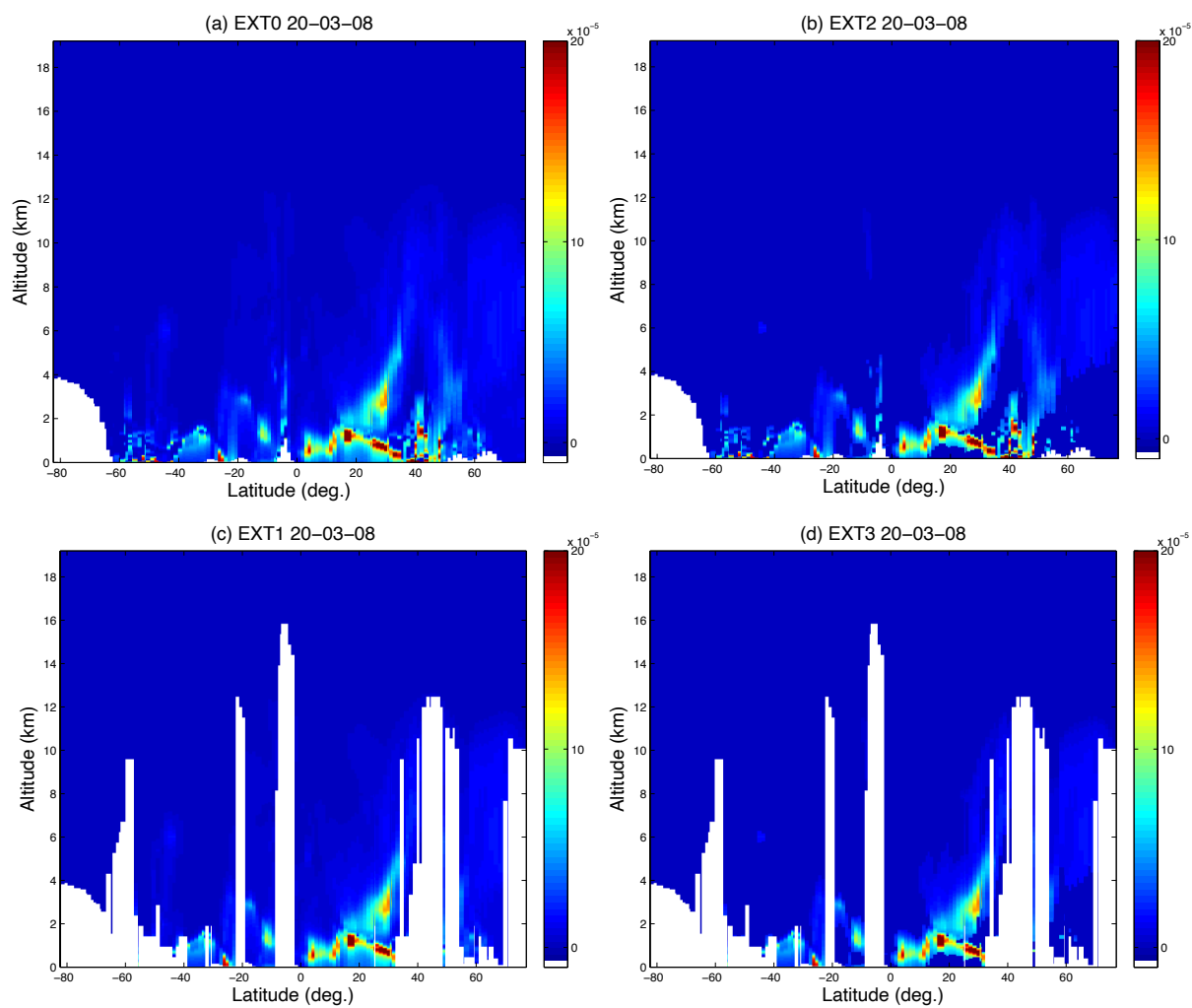
Figure 4 : Total extinction vertical profiles (m⁻¹) defined on 320 levels and calculated by the COSPv2 simulator along the satellite orbit on the 20-03-2008 : (a) Initial profiles EXT0; (b) Profiles with the instrument aerosol detectability threshold EXT2; (c) Cloud screened profiles EXT1; (d) Cloud screened profiles with aerosol detectability threshold applied EXT3

1
2
3
4
5
6
7
8
9
10
11
12
13
14
15
16
17
18
19
20
21
22
23
24
25
26
27
28
29
30

The vertical profiles of cloud fractions of Figure 3a are then defined at the horizontal sub-grid scale (with about 50 profiles being produced in each grid box), with values of cloud fraction being equal to 0 or 1 in each subgrid box. Vertically, the cloud fractions are interpolated on 40 levels, defined by their altitude. The resulting sub-profiles are shown in Figure 3b and are consistent with the model outputs of cloud cover of Figure 3a.

Finally, the aerosol optical properties α_a and β_a calculated by the E3SMv1 model at 532 nm along the satellite trajectory are used as inputs to the COSPv2 simulator. These quantities are calculated by the E3SM model at a very high vertical resolution, that reaches 90 m in the first 1.5 km above the ground level, and about 600 m between 1.5 km and 10 km. In the near future, the model vertical resolution will be even higher and reach 30 m in the first 3 km above the surface. The aerosol extinction and backscatter profiles show a very high correlation, with largest values below 800 hPa (Figures 3c and 3d).

The α_a profiles are then interpolated vertically on the 320 altitude levels to produce the EXT_0 variable (Figure 4a). The differences between the EXT_0 and EXT_2 fields (Figure 4b) illustrate the effect of applying the instrument aerosol detectability threshold. In the EXT_2 field, the values of the extinction coefficients that are lower than that threshold are set to zero. The extinction profiles thus appear less noisy in the middle troposphere (for example around 6 km at 20°S), whereas they remain similar in the lower troposphere. Finally the EXT_1 field (Figure 4c), shows the extinction profiles when the cloud screening is applied ; and the EXT_3 field (Figure 4d) both combines the cloud screening and the aerosol detectability threshold.

The resulting SR profiles computed by the COSPv2 simulator are shown in Figure 5. The obtained SR values, going up to 3 in maximum regions, agree well with the observations. South of 20°N, the signal above the detectability threshold (Figure 5b) is found below the altitude of 4 km, but north of 20°N, the aerosol plume extends vertically and a significant signal is found at altitudes as high as 12 km, in good agreement with the observations (Figure 2b).
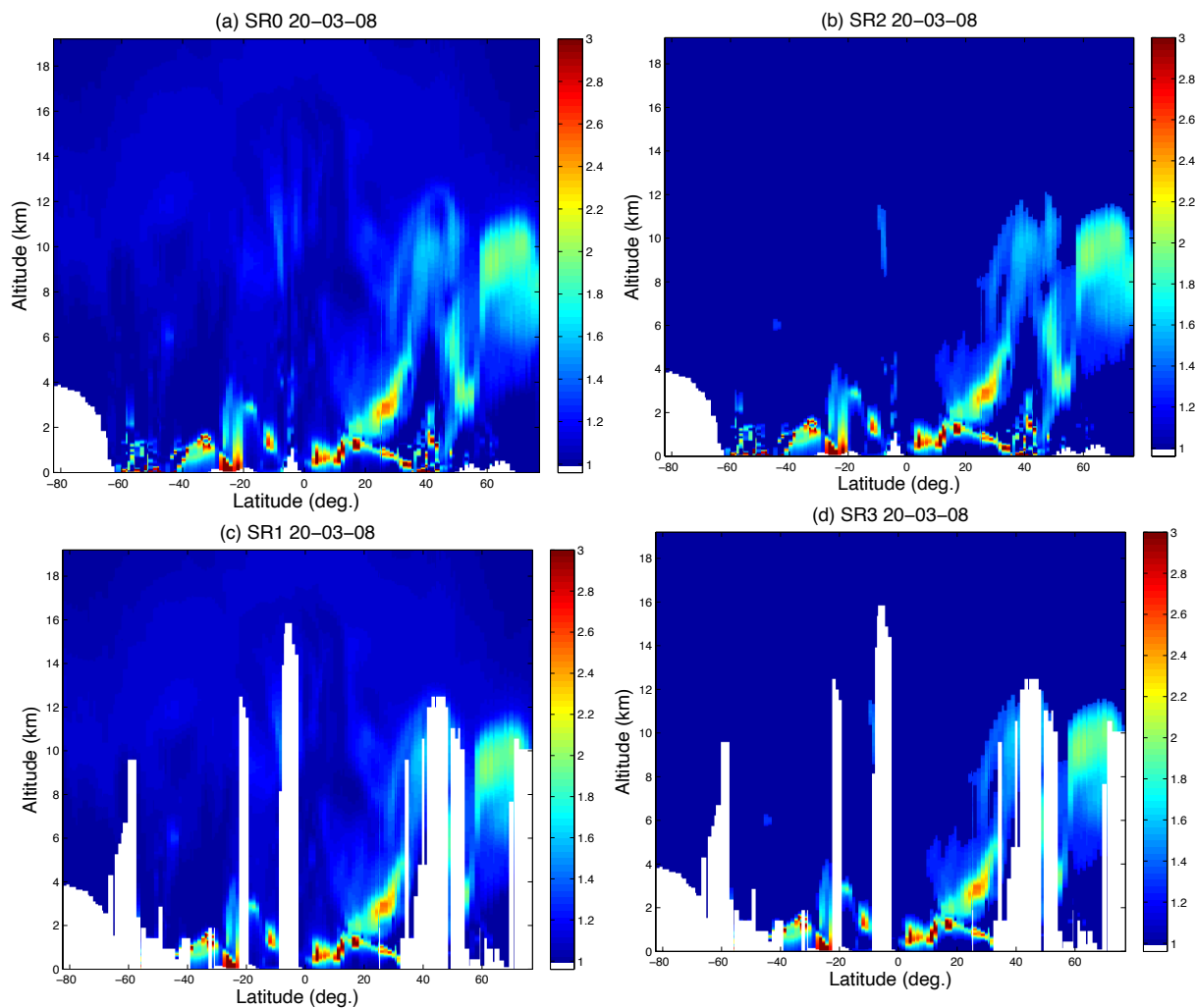
Figure 5 : Backscatter ratio vertical profiles defined on 320 levels and calculated by the COSPv2 simulator along the satellite orbit on the 20-03-2008 : (a) Initial profiles SR0; (b) Profiles with the instrument aerosol detectability threshold SR2; (c) Cloud screened profiles SR1; (d) Cloud screened profiles with aerosol detectability threshold applied SR3
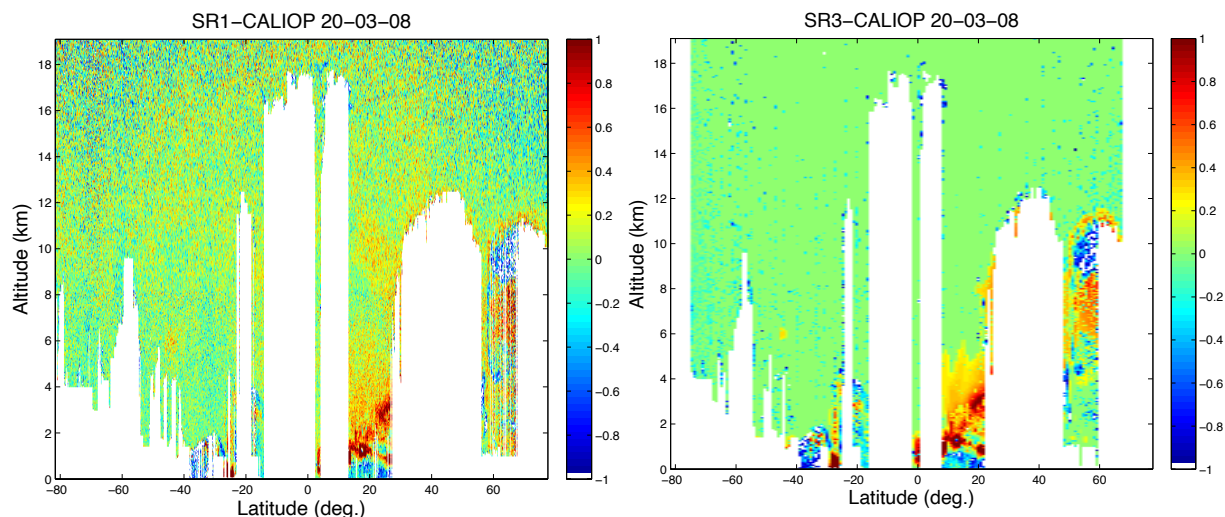
Figure 6 : (left) Difference between model SR1 and CALIOP data before data processing ; (right) Difference between model SR3 and CALIOP data after data processing (see text for details) along the satellite orbit on the 20-03-2008.
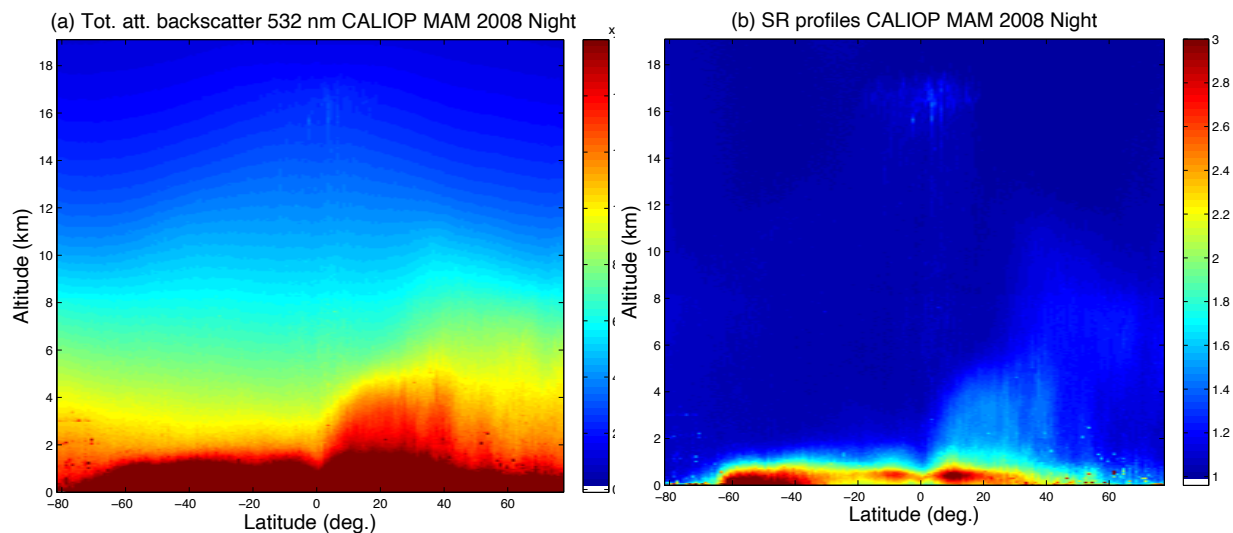
Figure 7 : (a) Attenuated total backscatter profiles (km^{-1}sr^{-1}) and backscatter ratio profiles (b) observed by CALIOP at 532 nm at night and averaged over longitudes and time during MAM 2008.

Figure 6 quantifies the differences between the simulated and observed SR values, before and after the applications of the AMB/SR thresholds. Figure 6a shows the differences between the SR1 field (with cloud screening only) and CALIOP profiles before applying the AMB/SR thresholds. In the upper troposphere, the instrument noise induces differences in absolute value that sometimes exceed 0.4. In Figure 6b, the differences between the SR3 field (with cloud screening and aerosol detectability threshold) and the CALIOP profiles after the thresholds application, become close to zero in the upper troposphere. The E3SMv1 model underestimates the aerosol concentrations near the surface around 30°S, but overestimates the concentrations in the aerosol plume north of 20°N between 1km and 9 km.

4.2 Global statistics

To have an overview of the aerosol distribution at the seasonal timescale, we average the observed and simulated ATB and SR profiles over three months: March, April and May (MAM) 2008. The thresholds on AMB and SR are applied to observations. The profiles are further averaged over all longitudes for each 1° latitude bin and are represented in Figure 7. The attenuated total backscatter signal, as the molecular backscatter signal (not shown), shows a decrease with altitude in the lower troposphere. The SR ratio, directly depending on aerosol concentrations, shows maxima reaching the value of 3 in the 2 km - layer above the surface. The ratios are especially large at 10°N and between 40°S and 60°S.

At 10°N, the maximum can be attributable to the presence of dust, that is the predominant component of aerosol over Northern Africa, the Arabian Peninsula and the Western China (Yu et al. 2010). Between 40°S and 60°S, the main aerosol contribution during the MAM season is sea spray, as biomass burning over Southern America and Southern Africa occurs mainly between June and November. The maximum between 40°S and 60°S also appears within the first kilometer above the surface on zonal mean 532 nm aerosol extinction profiles retrieved from CALIOP over the whole year during nighttime by Winker et al. (2013). The vertical extension of the aerosol plume seems to be largest in the Northern Hemisphere, where convection is the most active in MAM, whereas it is limited to the top of the boundary layer in the Southern Hemisphere, consistently with the scale heights retrieved by Yu et al. 2010.

The simulated SR3 profiles computed for the same period by the COSPv2 simulator are shown in Figure 8d. The maximum at 10°N is well reproduced, but the maximum in the Southern Hemisphere does not appear, which might be due to an inaccurate simulation of sea spray aerosols in the model at this time and location. As in the observations, the aerosol plume shows a larger vertical extension in the Northern Hemisphere than in the Southern Hemisphere, which validates the convective transport of aerosols in the model. Yu et al. (2010) expressed the concern that convective transport of aerosol could not be well retrieved by CALIOP observations because of the impossibility of retrieving concentrations in regions of thick convective clouds. However, the comparison between the SR0 (Figure 8a) and SR1 fields (Figure 8c) shows little differences, indicating that in the model, cloud screening does not affect
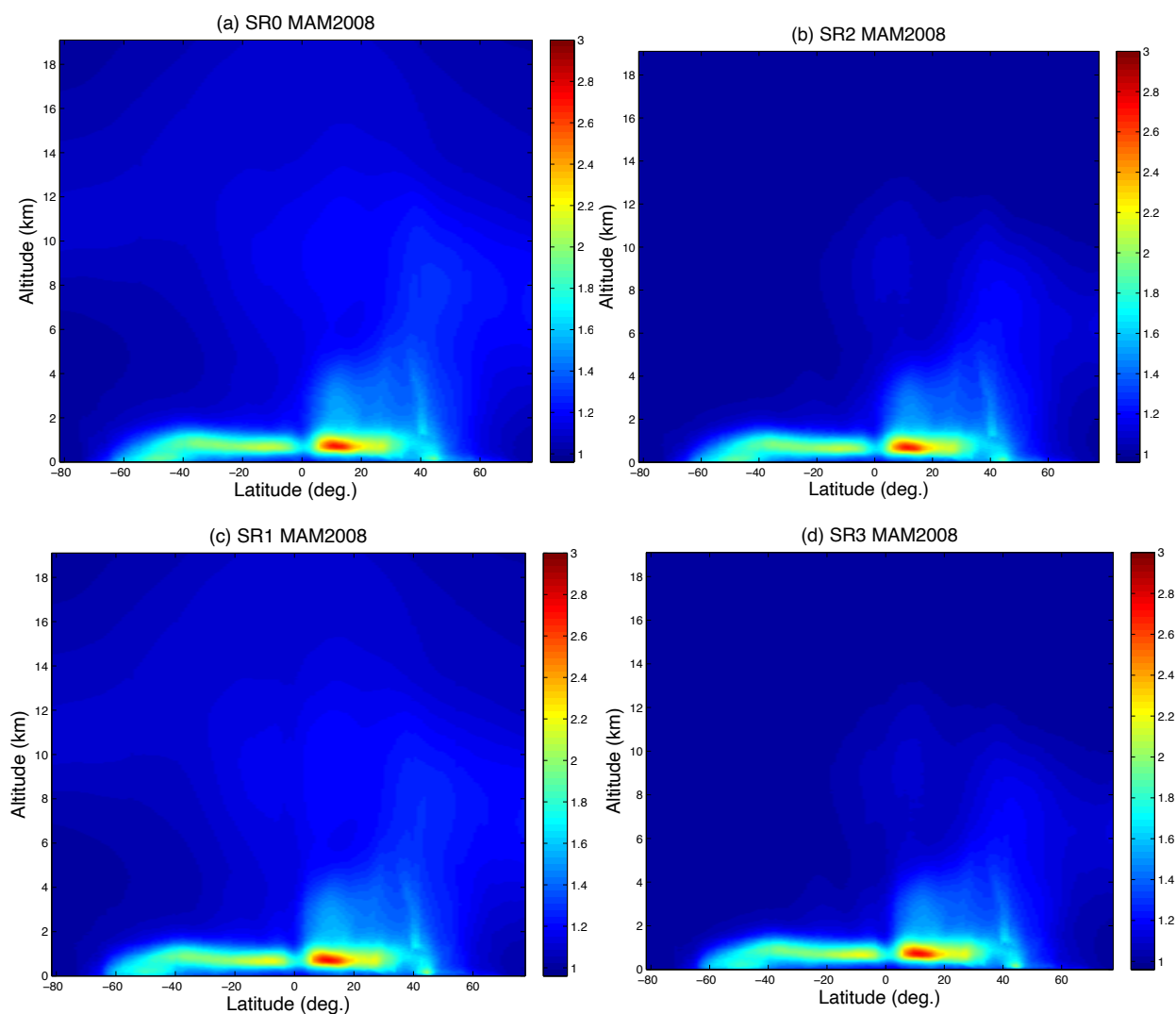
Figure 8 : SR profiles simulated by E3SMv1 at 532 nm and averaged over longitudes and time during MAM 2008 : (a) initial profiles SR0; (b) with the aerosol detectability threshold applied SR2; (c) cloud screened profiles SR1; (d) cloud screened profiles, with aerosol detectability threshold applied (SR3).

1   dramatically the mean aerosol concentrations and does not modify significantly the amount of aerosol

2   transported upward.

3

4   Finally, to compare quantitatively the simulated and observed SR values, we present in Figure 9 the

5   differences between the SR3 profiles and the CALIOP SR profiles after the application of the AMB/SR

6   thresholds (see Section 3) in the first 4 km above the surface. The SR maxima are underestimated by 1

7   to 1.5 in the model from the surface to 500-800 m, and are slightly overestimated above this level up to

8   1.5-1.8 km. The underestimation of SR in the surface layer corresponds to a relative model error on the

9   aerosol optical depth of approximately 50%. This vertical distribution bias revealed by the simulator

10 could have several causes that need to be investigated further, as a vertical mixing or a convective
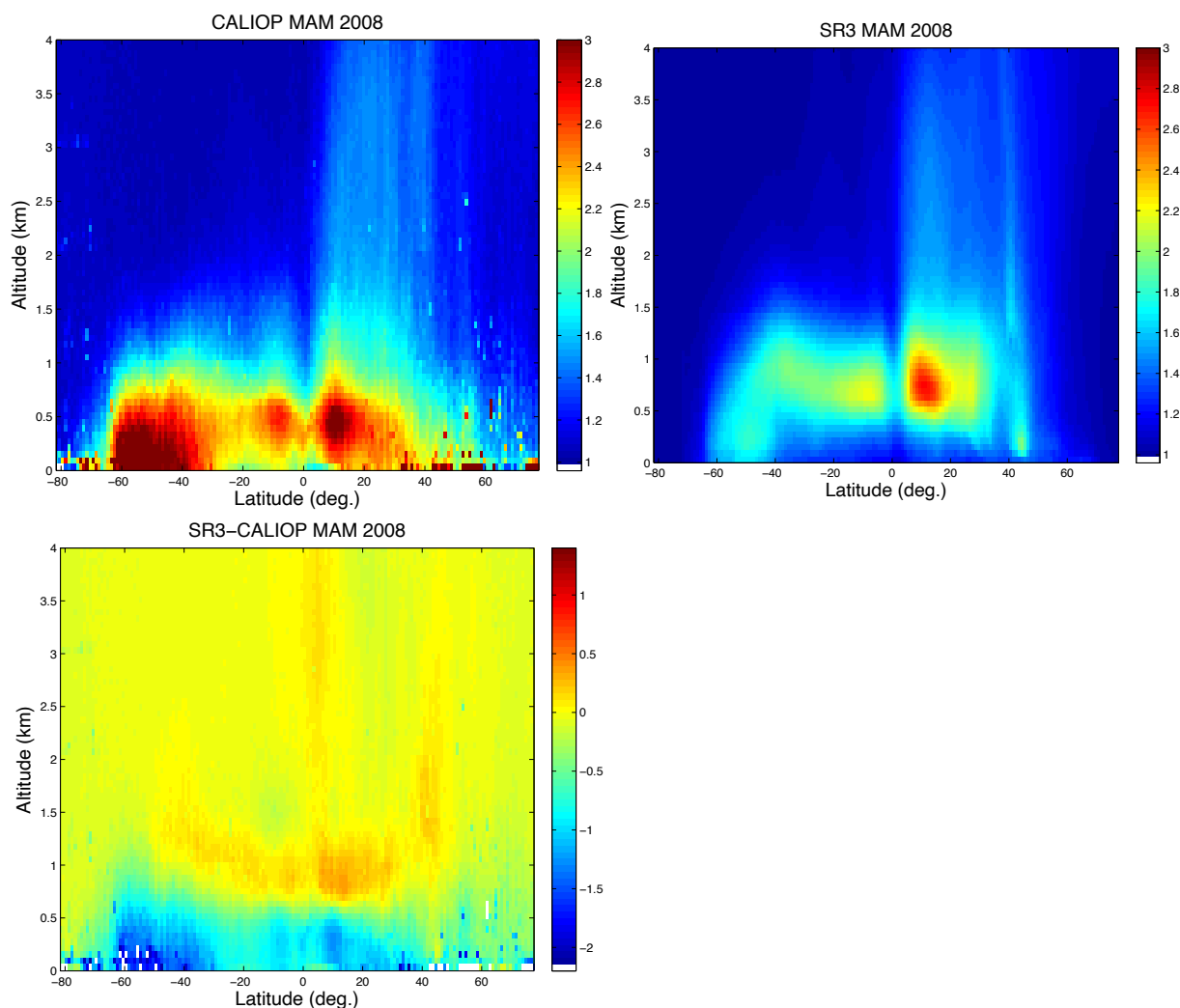
11

Figure 9 : Up left : CALIOP SR after data processing (see text for details) ; Up right : Model SR3 ; Bottom : Difference between model SR3 and CALIOP SR. All fields are shown between 0 and 4 km and are averaged over all longitudes and time during MAM 2008.

transport that would be too efficient, or a wet scavenging that would be incorrect in the E3SMv1 model.

5. Discussion

A cause of the discrepancy between simulated SR3 fields and SR fields retrieved from CALIOP observations can be due to the differences between model and observed clouds. For those two fields corresponding to cloud-free conditions only, the differences in the occurrences of cloud-free cases in the model and observations can affect the sampling of aerosol concentrations. If those aerosol concentrations show a large spatiotemporal variability, differences in sampling can induce differences in the seasonal or zonal mean concentrations, and thus in the mean SR.

17

To compare the sampling induced by the cloud-screening in E3SMv1 and in CALIOP, we consider the probability of having cloud-free conditions during the night at a daily scale in 1°x1° horizontal grid cells at a given latitude, during the MAM period (Figure 10a). In the observations, the total cloud cover CLT is estimated in the 532 nm channel of CALIOP. The probabilities for cloud-free conditions (CLT=0%) at nighttime are extremely low in CALIOP for all latitudes, except for polar regions that are dry and less cloudy than the rest of the globe (especially over land). Probabilities are much higher in CESM, with a maximum value of 70% in the Southern polar region, and maximum values of almost 40% and 50% at 25°S and 25°N, respectively.

However the cloud-free grid cells are not the only ones to be sampled for the estimation of the mean SR during the MAM period. The grid cells with a partial cloud cover (0<CLT<100%) are also associated with a daily SR value, that is computed in the clear-sky sub-columns of the considered grid cell in CESM, and retrieved within the cloud-free pixels belonging to the grid cell for CALIOP. Making the reasonable assumption that aerosol concentrations are homogeneous within the 1°x1° grid, this local estimation of SR can be considered to be representative of the whole grid cell.

The probabilities of partially covered grid cells (shown in Figure 10b) are everywhere higher in CALIOP observations that in the CESM model. In CALIOP, the probabilities show two maxima of about 70% in the subtropical regions, while they are not above 50% in E3SMv1 at these latitudes.

If the probability for having CLT<100% was equal to 100% both in model and observations (no overcast grid-boxes in either model or observations), then the sampling would be perfect, with the totality of the grid cells equally contributing to the estimations of the observed and modeled mean SR values for the MAM period. However, the sum of the cloud-free probability (Figure 10a) and the partial cloud cover probability (Figure 10b) is lower than 100%, both in E3SMv1 and in CALIOP. We thus finally consider in Figure 10c the probability of having fully overcast grid cells (CLT=100%) as a function of latitude. These grid cells are totally filtered out and thus do not contribute to the estimations of the mean SR values. Probabilities are highest at 60°S both in E3SMv1 (80%) and in CALIOP observations (65%) during the MAM period. Maxima of lower amplitude are also found in the equatorial region and in middle and high latitudes in the Northern Hemisphere. The probabilities are almost everywhere overestimated by the model, that tends to produce more extreme cloud cover cases (0% or 100%) than in the observations.

The very large occurrences of overcast cases at 60°S suggest that the sampling of SR values in both simulations and observations after cloud-screening at this latitude might not be representative of the whole time period and of whole longitudes. Large sampling errors can then be inferred on the mean SR values at 60°S if the SR fields show a large spatiotemporal variability at this latitude. Errors might also arise in the Equatorial region and in the Northern Hemisphere at middle latitudes, where the occurrences of fully covered cases are high, or in the Northern polar region, where occurrences are significantly different in observations and simulations.

Of course, the occurrences of overcast cases depend on the size of the horizontal grid cells, and decrease with a coarser resolution. For example, the probability of having CLT=100% does not exceed
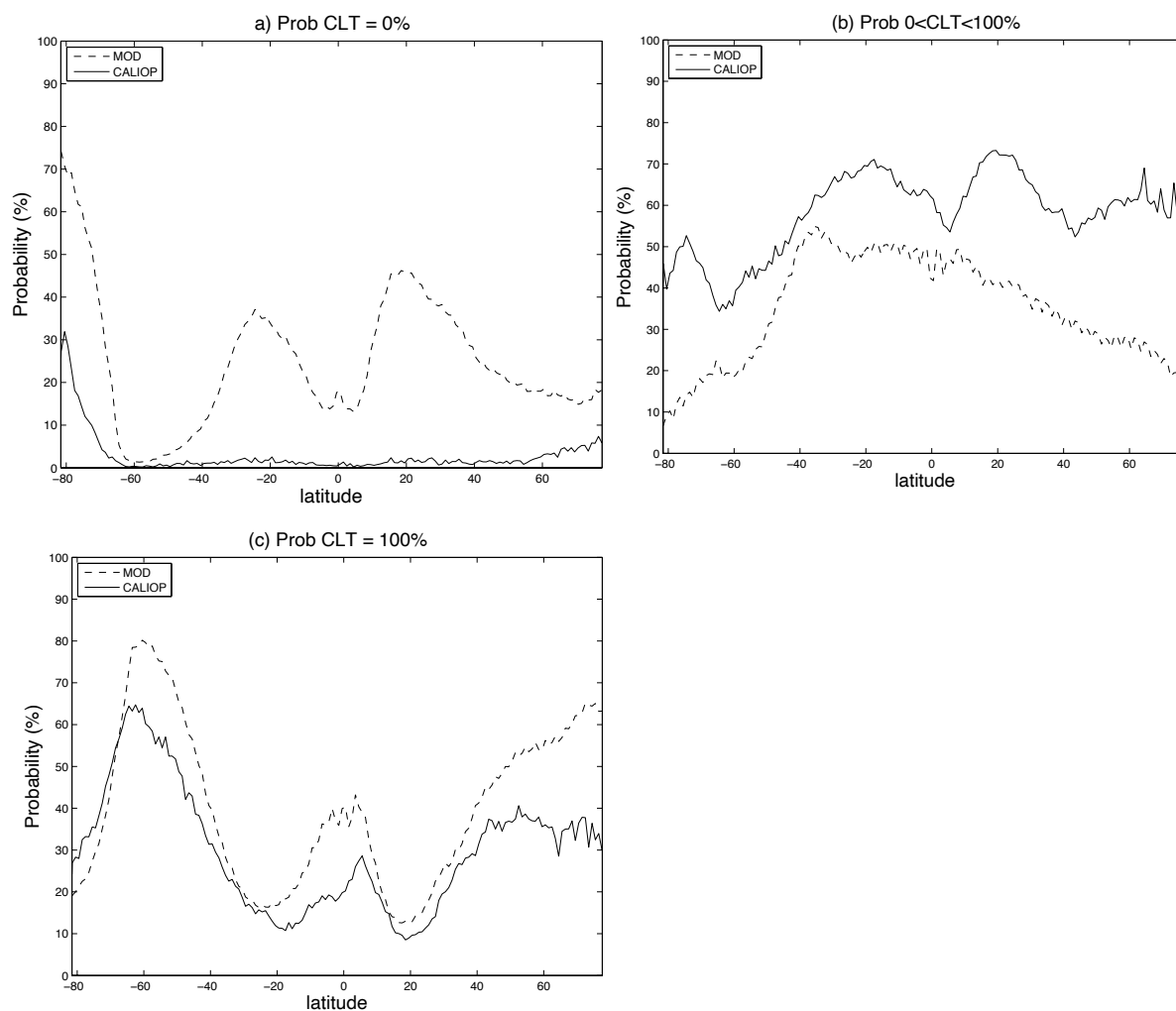
Figure 10 : (a) Probabilities of (a) cloudy-free; (b) partially cloud covered; (c) totally cloud covered 1ºx1º horizontal grid cells as a function of latitude, during the MAM period (nighttime), in CALIOP and E3SMv1.

1   5% at 60ºS for 10ºx10º horizontal grid cells (not shown). Choosing a coarser resolution might then

2   ensure a better temporal sampling, but on the other hand, taking account of the partially covered

3   10ºx10º grid cells for the mean SR estimation would be based on the implicit assumption that the

4   aerosol concentrations are homogeneous over these grid cells of large horizontal surfaces, which is

5   probably not realistic in the vicinity of the source regions.

6

7

8
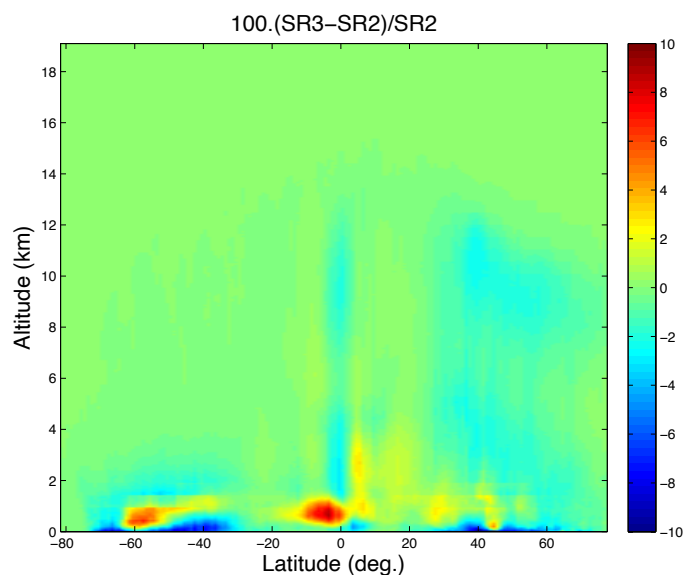
Figure 11 : Relative difference (in %) between the SR3 field and the SR2 field both computed by E3SMv1, as a function of latitude and altitude.

1   To measure the impact of the cloud screening on the mean SR values in simulations, we compute the

2   relative difference between the SR3 field (with both aerosol detectability threshold and cloud screening

3   applied) and the SR2 field (with the detectability threshold applied and no cloud-screening). This rela-

4   tive difference, shown in Figure 11 as a function of altitude and latitude, is everywhere lower than 10%

5   in absolute value. In regions where cloud screening is large in the model (for example at 60°S and in

6   the Equatorial region) SR3 values tend to be larger than SR2 values, probably because most of the SR2

7   profiles correspond to cloud and rainfall conditions, while SR3 profiles correspond to dry cases only,

8   and thus cloud screened aerosol concentrations are higher because wet scavenging does not occur.

9   Furthermore the low absolute values of relative differences in Figure 11 imply that the intra-seasonal

10   variability of aerosol emissions is low in the model. This variability depends on the emissions of an-

11   thropogenic aerosols, that are monthly mean averaged, consistently across all CMIP6 models (Hoesly

12   et al (2018) and van Marle et al (2017)). It also depends on the variability of sea spray aerosol emis-

13   sions, that somewhat follows the variability of surface winds and SST.

14

15   Overall, the poor sampling induced at some locations by cloud-screening does not impact significantly

16   the mean SR values in E3SMv1, and consequently, errors in E3SMv1 clouds cannot impact the aerosol

17   seasonal comparison between E3SMv1 and CALIOP observations. In particular, the large difference

18   observed at 60°S between the observed and simulated mean SR values cannot be explained by the large

19   cloud-screening in E3SMv1 at this latitude.

20

21   Nevertheless, cloud-screening might have a larger impact on the mean aerosol CALIOP retrievals.

22   Winker et al. (2013) found a lack of correlation between high semi-transparent cloud and aerosol in the

23   lower troposphere in most regions in CALIOP data, implying that the screening of thin clouds does not

24   significantly impact the retrieved values of AOD or aerosol extinction coefficients. However this result

25

1 has to be extended to opaque cloud screening and has to be examined over a three-month period at the
2 specific locations that exhibit large cloud covers. To get an insight into the representativeness of our SR
3 values retrieved from CALIOP, we computed the zonal mean SR values over the MAM period, by only
4 considering one third of the CALIOP data. We found that the relative differences between these SR
5 values and those obtained by using the totality of the available CALIOP data are highest in covered
6 regions, but never exceed 15% (not shown). This gives us confidence about the robustness of our re-
7 sults retrieved by CALIOP over a three-month period. An alternative approach would be to extend the
8 statistics to several years, but the results would then be affected by the inter annual variability of
9 aerosol concentrations.

10

11 We can thus conclude that :
12 1) the SR maxima retrieved by CALIOP over three months are robust, and
13 2) the method of comparison between the modeled and retrieved SR is robust, although the modeled
14 and observed clouds show large differences, because the areas of largest differences in cloud cover are
15 associated with a low variability of aerosol concentrations.

16

17 Consequently, the differences between observed and simulated SR values are directly attributable to the
18 aerosol representation in the model. Aerosol modeling basically consists of four elements, that are the
19 representation of aerosol sources, aerosol optics, aerosol chemistry and aerosol transport.

20

21 In the E3SMv1 model, aerosol optics is parameterized in terms of wet refractive index and wet surface
22 mode radius of each mode (Ghan and Zaveri, 2007). It assumes volume mixing to compute the wet
23 refractive index for mixtures of insoluble and soluble particles. The parameterization provides the
24 aerosol extinction α_a. We apply the same Ghan and Zaveri (2007) methodology to add the diagnostic
25 variable of the 180° backscatter β_a, as the aerosol lidar simulator requires these two input variables.
26 Most GCMs compute the aerosol extinction, but not many of them routinely compute the aerosol 180°
27 backscatter β_a. Hence, more work has to be done so that other GCMs also diagnose their aerosol 180°
28 backscatter β_a in a way that is consistent with their aerosol optics parameterization. For future compar-
29 isons between CALIOP data and other GCMs, or for model-to-model comparisons, one might find use-
30 ful to use one single optics module, to eliminate aerosol optics as a potential source of discrepancy in
31 the comparisons. This is beyond the scope of this study and requires future investigation.

32

33 To evaluate the representation of aerosol sources in the model, the NASA product providing aerosol
34 types from CALIPSO data is of particular interest. Indeed CALIOP level 2 data include seven aerosol
35 classes: clean marine, dust, polluted continental, clean continental, polluted dust, smoke, other. This
36 classification utilizes depolarization ratio, integrated attenuated backscatter coefficient, altitude, and
37 land vs ocean (Kim et al., 2018). The aerosol subtypes of CALIOP measurements have been compared
38 with daily aerosol types derived from AERONET level 2.0 inversion data by Mielonen et al., 2009 and
39 have been shown to be in agreement by 70%.

40

41 The CALIOP classification might be useful to point out more precisely the inaccuracies in the model
42 aerosol sources. According to this classification, the aerosol observed at 60°S during MAM is mostly
43 clean marine. The large differences observed between CALIOP and E3SMv1 at this latitude may then

be due to model biases in simulating marine aerosols in this region. Fig 9 in Rasch et al (2019) and Fig 11 in Wang et al (2020) also show an aerosol bias over the Southern Ocean. There are certainly many possible reasons. The E3SMv1 model has both sea salt and marine organics as marine aerosols. Their "emissions" are function of surface winds and SST, based on Martensson et al., 2003. The model has significant surface wind bias, that may thus impact the marine aerosol sources. Furthermore, McCoy et al (2021) shows that new particle formation (NPF) might be important in that region when they contrast SOCRATES field campaign measurements and CAM6 simulations. This process is not well represented in the CAM6 model or in the E3SM model. We demonstrate here that the aerosol lidar simulator is very useful in revealing these model biases, providing insights into future model development directions.

6. Perspectives

The validation of aerosols simulated by GCMs with space lidar data will be expanded to other lidars and to other GCMs. We plan to perform studies with the Laboratoire de Météorologie Dynamique Zoom (LMDZ) model, the European Center - HAMburg (ECHAM) model and the ICOsahedral Non-hydrostatic (ICON) model. The modal aerosol module "HAM" that employs seven log-normal aerosol modes is used interactively in the ECHAM model since almost two decades (Zhang et al. 2012 ; Tegen et al. 2019). Recently it is also implemented in the successor of ECHAM, the ICON model (Salzmann et al. 2022). The two models with profoundly different dynamical cores share the same physics package. It will be interesting to evaluate the differences induced by the two numerical representations of the atmospheric dynamics with the satellite retrievals.

Note that for a multi-model comparison, it is necessary to use a standard vertical grid with a coarser vertical resolution than N=320 levels and $\Delta z = 60$m, as traditional climate models do not reach such a fine resolution. For the comparison of these models with CALIOP observations, data interpolation is needed on the same vertical coarser grid. Vertically averaging the CALIOP data would enhance the SNR, and consequently would allow to lower the aerosols detectability threshold and make use of the more noisy CALIOP daily data. For each model it is important to check that the errors in the model clouds do not significantly impact the model-observation aerosol comparison over the considered period.

Since 2018, the ADM-Aeolus mission has been operating the first High-Spectral Resolution Lidar (HSRL) in space. Although primarily dedicated to wind measurements, the HSRL capability in the UV allows the separation of the molecular and particulate contributions and enables the measurements of the particulate backscatter and extinction coefficients. These measurements provide new insight of very thin aerosol layers and can be very useful for the validation of models that directly compute these quantities. Later in 2023, the EarthCare mission will also provide data from the HSRL lidar ATLID at 355 nm. The COSPv2 simulator can be easily adapted to other wavelengths, which opens the way to the determination of new diagnostics for cloud susceptibility, aerosol typing and aerosol-cloud proximity metrics.

7. Code and data avaibility

References

Cesana G., and H. Chepfer : How well do climate models simulate cloud vertical structure? a comparison between CALIPSO-GOCCP satellite observations and CMIP5 models, Geophys. Res. Let., 39, 20, doi:10.1029/2012GL053153, 2012.

Cesana G. and H. Chepfer : Evaluation of the cloud water phase in a climate model using CALIPSO-GOCCP, J. Geophys. Res., DOI: 10.1002/jgrd.50376, 2013.

Chepfer H., S. Bony, D. Winker, M. Chiriaco, J-L. Dufresne, G. Sèze : Use of CALIPSO lidar observations to evaluate the cloudiness simulated by a climate model, Geophys. Res. Let., 35, L15704, doi:10.1029/2008GL034207, 2008.

Costantino, L. and Bréon, F.-M.: Aerosol indirect effect on warm clouds over South-East Atlantic, from co-located MODIS and CALIPSO observations, Atmos. Chem. Phys., 13, 69–88, https://doi.org/ 10.5194/acp-13-69-2013, 2013.

1 Douville, H., K. Raghavan, J. Renwick, R.P. Allan, P.A. Arias, M. Barlow, R. Cerezo-Mota, A. Cherchi,
2 T.Y. Gan, J. Gergis, D. Jiang, A. Khan, W. Pokam Mba, D. Rosenfeld, J. Tierney, and O. Zolina : Water
3 Cycle Changes. In Climate Change : The Physical Science Basis. Contribution of Working Group I to
4 the Sixth Assessment Report of the Intergovernmental Panel on Climate Change [Masson-Delmotte, V.,
5 P. Zhai, A. Pirani, S.L. Connors, C. Péan, S. Berger, N. Caud, Y. Chen, L. Goldfarb, M.I. Gomis, M.
6 Huang, K. Leitzell, E. Lonnoy, J.B.R. Matthews, T.K. Maycock, T. Waterfield, O. Yelekçi, R. Yu, and
7 B. Zhou (eds.)]. Cambridge University Press. In Press, 2021.

8 Forster, P., T. Storelvmo, K. Armour, W. Collins, J.-L. Dufresne, D. Frame, D.J. Lunt, T. Mauritsen,
9 M.D. Palmer, M. Watanabe, M. Wild, and H. Zhang: The Earth's Energy Budget, Climate Feedbacks,
10 and Climate Sensitivity. In Climate Change 2021: The Physical Science Basis. Contribution of Work-
11 ing Group I to the Sixth Assessment Report of the Intergovernmental Panel on Climate Change [Mas-
12 son-Delmotte, V., P. Zhai, A. Pirani, S.L. Connors, C. Péan, S. Berger, N. Caud, Y. Chen, L. Goldfarb,
13 M.I. Gomis, M. Huang, K. Leitzell, E. Lonnoy, J.B.R. Matthews, T.K. Maycock, T. Waterfield, O.
14 Yelekçi, R. Yu, and B. Zhou (eds.)]. Cambridge University Press. In Press, 2021.

15 Gelaro, R., McCarty, W., Suárez, M. J., Todling, R., Molod, A., Takacs, L., Randles, C. A., Darmenov,
16 A., Bosilovich, M. G., Reichle, R., et al.: The modern-era retrospective analysis for research and ap-
17 plications, version 2 (MERRA-2), Journal of climate, 30, 5419–5454, 2017.

18
19 Golaz et al. : https://agupubs.onlinelibrary.wiley.com/doi/full/10.1029/2018MS001603, 2019.

20 Guzman, R., Chepfer, H., Noel, V., Vaillant de Guelis, T., Kay, J.E., Raberanto, P., Cesana, G.,
21 Vaughan, M. A., and D. M. Winker : Direct atmosphere opacity observations from CALIPSO provide
22 new constraints on cloud-radiation interactions, J. Geophys. Res. Atmos., DOI:
23 10.1002/2016JD025946, 2017.

24 Hodzic A., H. Chepfer, R. Vautard, P. Chazette, M. Beekmann, B. Bessagnet, P. Drobinski, P. Goloub,
25 M. Haeffelin, Y. Morille, B. Chatenet, J. Cuesta : Comparisons of aerosol chemistry-transport model
26 simulations with lidar and sun-photometer observations at a site near Paris, J. Geophys.Res.t., 109,
27 D23201, doi: 10.1029/2004JD004735, 2004.

28 Hoesly, R. M., S. J. Smith, L. Feng, Z. Klimont, G. Janssens-Maenhout, T. Pitkanen, J. J. Seibert, L.
29 Vu, R. J. Andres, R. M. Bolt, T. C. Bond, L. Dawidowski, N. Kholod, J. Kurokawa, M. Li, L. Liu, Z.
30 Lu, M.C. Moura, P. R. O'Rourke, and Q. Zhang : Historical (1750-2014) anthropogenic emissions of
31 reactive gases and aerosols from the Community Emissions Data System (CEDS), Geoscientific Model
32 Development, Vol. 11, issue 1, pp 369-408, 2018.

33 Keating, T., and A. Zuber, Hemispheric transport of air pollution, Air Pollution Studies 16, 2007.

34 Kim, M.-H., A. H. Omar, J. L. Tackett, M. A. Vaughan, D. M. Winker, C. R. Trepte, Y. Hu, Z. Liu, L.
35 R. Poole, M. C. Pitts, J. Kar and B. E. Magill : "The CALIPSO Version 4 Automated Aerosol Classific-
36 ation and Lidar Ratio Selection Algorithm", Atmos. Meas. Tech., 11, 6107-6135, https://doi.org/
37 10.5194/amt-11-6107-2018, 2018.

38 Koch, D., and A.D. Del Genio : Black carbon absorption effects on cloud cover: Review and
39 synthesis. Atmos. Chem. Phys., 10, 7685-7696, doi:10.5194/acp-10-7685-2010, 2010.

40 Koffi, B., et al. : Application of the CALIOP layer product to evaluate the vertical distribution of aero-
41 sols estimated by global models: AeroCom phase I results, J. Geophys. Res., 117, D10201,
42 doi:10.1029/2011JD016858, 2012.

43

Koffi, B., et al. : Evaluation of the aerosol vertical distribution in global aerosol models through comparison against CALIOP measurements: AeroCom phase II results, J. Geophys. Res. Atmos.,121, 7254– 7283, doi:10.1002/2015JD024639, 2016.

Ma et al. : https://acp.copernicus.org/articles/14/8631/2014/, 2015.

Ma, P-L., P. Rasch, H. Chepfer, D. Winker, and S. Ghan : Observational Constraint on Cloud Susceptibility Weakened by Aerosol Retrieval Limitations, Nature Communication, 9, 2640, 2018.

Martensson, E. M., E. D. Nilsson, G. de Leeuw, L. H. Cohen, H-C Hansson : Laboratory simulations and parameterization of the primary marine aerosol production, Journal of Geophysical Research-Atmospheres, Vol. 108, Issue D9, 2003.

Mielonen, T. , A. Arola, M. Komppula, J. Kukkonen, J. Koskinen, G. de Leeuw, K. E. J. Lehtinen : Comparison of CALIOP level 2 aerosol subtypes to aerosol types derived from AERONET inversion data, Geophysical Research Letters, Vol. 36, Issue 18, 2009.

Quaas, J., A. Arola, B. Cairns, M. Christensen, H. Deneke, A. M. L. Ekman, G. Feigold, A. Fridlind, E. Gryspeerdt, O. Hasekamp, Z. Li, A. Lipponen, P.-L. Ma, J. Mülmenstädt, A. Nenes, J. Penner, D. Rosenfeld, R. Schrödner, K. Sinclair, O. Sourdeval, P. Stier, M. Tesche, B. Van Diedenhoven, and M. Wendisch, Constraining the Twomey effect from satellite observations: Issues and perspectives, Atmos. Chem. Phys., 20, 15079-15099, doi:10.5194/acp-20-15079-2020, 2020.

Rasch P. J., S. Xie, P.-L. Ma, W. Lin, H. Wang, Q. Tang, S. M. Burrows, P. Caldwell, K. Zhang, R. C. Easter, P. Cameron-Smith, B. Singh, H. Wan, J.-C. Golaz, B. E. Harrop, E. Roesler, J. Bacmeister, V. E. Larson, K. J. Evans, Y. Qian, M. Taylor, L. R. Leung, Y. Zhang, L. Brent, M. Branstetter, C. Hannay, S. Mahajan, A. Mametjanov, R. Neale, J. H. Richter, J.-H. Yoon, C. S. Zender, D. Bader, M. Flanner, J. G. Foucar, R. Jacob, N. Keen, S. A. Klein, X. Liu, A.G. Salinger, M. Shrivastava, Y. Yang : An Overview of the Atmospheric Component of the Energy Exascale Earth System Model, Journal of Advances in Modeling Earth Systems, Vol. 11, Issue 8, pp 2377-2411, 2019.

Reverdy, M., H. Chepfer, D. Donovan, V.Noel, G. Cesana, C.Hoareau,M. Chiriaco, and S. Bastin (2015), An EarthCARE/ATLID simulator to evaluate cloud description in climate models, J. Geophys. Res. Atmos., 120, 11,090–11,113, doi:10.1002/ 2015JD023919, 2015.

Salzmann, M., et al., The global atmosphere-aerosol model ICON-A-HAM2.3 -- Initial model evaluation and effects of radiation balance tuning on aerosol optical thickness. J. Adv. Model. Earth Syst., in press, 2022.

Stier, P.: Limitations of passive remote sensing to constrain global cloud condensation nuclei, Atmos. Chem. Phys., 16, 6595–6607, https://doi.org/10.5194/acp-16-6595-2016, 2016.

Stromatas S., S. Turquety, L. Menut, H. Chepfer, G. Cesana, J.-C. Pere, and B. Bessagnet : Lidar Signal Simulation for the Evaluation of Aerosols in Chemistry-Transport Models, Geoscientific Model Development, Geosci. Model Dev., 5, 1543-1564, doi:10.5194/gmd-5-1543-2012, 2012.

Szopa, S., V. Naik, B. Adhikary, P. Artaxo, T. Berntsen, W.D. Collins, S. Fuzzi, L. Gallardo, A. Kiendler Scharr, Z. Klimont, H. Liao, N. Unger, and P. Zanis : Short-Lived Climate Forcers. In Climate Change 2021: The Physical Science Basis. Contribution of Working Group I to the Sixth Assessment Report of the Intergovernmental Panel on Climate Change [Masson-Delmotte, V., P. Zhai, A. Pirani, S.L. Connors, C. Péan, S. Berger, N. Caud, Y. Chen, L. Goldfarb, M.I. Gomis, M. Huang, K. Leitzell, E. Lonnoy, J.B.R. Matthews, T.K. Maycock, T. Waterfield, O. Yelekçi, R. Yu, and B. Zhou (eds.)]. Cambridge University Press. In Press., 2021.

Tegen, I., Neubauer, D., Ferrachat, S., Siegenthaler-Le Drian, C., Bey, I., Schutgens, N., Stier, P., Watson-Parris, D., Stanelle, T., Schmidt, H., Rast, S., Kokkola, H., Schultz, M., Schroeder, S., Daskalakis, N., Barthel, S., Heinold, B., and Lohmann, U.: The global aerosol–climate model ECHAM6.3–HAM2.3 – Part 1: Aerosol evaluation, Geosci. Model Dev., 12, 1643–1677, https://doi.org/10.5194/gmd-12-1643-2019, 2019.

Van Marle, M. J. E., S. Kloster, B. I. Magi, J. R. Marlon, A-L. Daniau, R. D. Field, A. Arneth, M. Forrest, S. Hantson, N. M. Kehrwald, W. Knorr, G. Lasslop, F. Li, S. Mangeon, C. Yue, J. W. Kaiser, and G. R. van der Werf : Historic global biomass burning emissions for CMIP6 (BB4CMIP) based on merging satellite observations with proxies and fire models (1750–2015), Geoscientific Model Development, Vol. 10, issue 9, pp 3329-3357, 2017.

Vuolo, M. R., H. Chepfer, L. Menut, and G. Cesana : Comparison of mineral dust layers vertical structures modelled with Chimere-Dust and observed with the Caliop lidar., J. Geophys. Res., doi:10.1029/2008JD011219, 2009.

Waquet, F. , J. Riedi, L. C. Labonnote, P. Goloub, B. Cairns, J-L Deuzé, and D. Tanré : Aeorosol Remote Sensing over Clouds Using A-Train Observations, Journal of the Atmospheric Sciences, Vol. 66 : Issue 18, pp 2468-2480, 2009.

Winker, D. M., J. L. Tackett, B. J. Getzewich, Z. Liu, M. A. Vaughan, and R.R. Rogers : The Global 3-D distribution of tropospheric aerosols as characterized by CALIOP, Atmospheric Chemistry and Physics, Vol. 13, issue 6, 2013.

Yu, H., M. Chin, D. M. Winker, A. H. Omar, Z. Liu, C. Kittaka and T. Diehl : Global view of aerosol vertical distributions from CALIPSO lidar measurements and GOCART simulations : Regional and seasonal variations, Journal of Geophysical Research-Atmospheres, Vol. 115, Issue D4, 2010.

Zarzycki, M. and T. C. Bond, How much can the vertical distribution of black carbon affect its global direct radiative forcing?, Geophysical Research Letters, Vol. 37, Issue 20 : https://doi.org/10.1029/2010GL044555, 2010.

Zhang, K., D. O'Donnell, J. Kazil, P. Stier, S. Kinne, U. Lohmann, S. Ferrachat, B. Croft, J. Quaas, H. Wan, S. Rast, and J. Feichter, The global aerosol-climate model ECHAM5-HAM, version 2: sensitivity to improvements in process representations, Atmos. Chem. Phys., 12, 8911-8949, doi:10.5194/acp-12-8911-2012, 2012.

Watson-Parris, D., N. Schutgens, D. Winker, S.P. Burton, R.A. Ferrare and P. Stier, On the limits of CALIOP for constraining modeled, free tropospheric aerosol, Geophys. Res. Let., Vol. 45, Issue 17, 9260-9266, https://doi.org/10.1029/2018GL078195, 2018.

Zhang et al.: https://agupubs.onlinelibrary.wiley.com/doi/full/10.1002/2015GL064183, 2014.